Journal of Molecular Graphics and Modelling 29 (2010) 295–308

Contents lists available at ScienceDirect

Journal of Molecular Graphics and Modelling

journal homepage: www.elsevier.com/locate/JMGM

Computational and mutagenesis studies of the streptavidin native dimer interface

Cheng-Kuo Hsu, Sheldon Park*

Department of Chemical and Biological Engineering, University at Buffalo, Buffalo, NY 14260, United States

ARTICLE INFO

Article history:
Received 27 March 2010
Received in revised form 8 August 2010
Accepted 15 September 2010
Available online 30 October 2010

Keywords:
Streptavidin
Quaternary structure
Molecular dynamics simulation
Solvent accessible surface area
Knob-into-hole interaction

ABSTRACT

Wt streptavidin forms a domain swapped tetramer consisting of two native dimers. The role of tetramerization has been studied previously and is known to contribute to biotin binding by allowing the exchange of W120 between adjacent subunits. However, the role of dimer formation in streptavidin folding and function has been largely overlooked to date, although native dimers are necessary for tetramer formation and thus for high affinity biotin binding. To understand how the side chain interactions at the dimer interface stabilize the subunit association, we studied the structural and functional consequences of introducing interfacial mutations by a combination of molecular dynamics (MD) simulation and biochemical characterization. In particular, we introduced rational mutations at the dimer interface to engineer new side chain interactions and measured the stability and function of the resulting mutants. We focused on two residues that form a "knob" and a "hole" pair, G74 and T76, since steric complementarity plays an important role at these positions. We introduced mutations that would change the polarity and side chain packing to test if the interface can be rationally redesigned. Both energy calculation and geometric parameterization were used to interpret the simulated structures and predict how the mutations affect the dimer stability. In this regard, obtaining precise energy estimates was difficult because the simulated structures have large stochastic variations and some mutants did not reach an equilibrium by the end of the simulation. In contrast, comparing the wt and mutants to one another and parameterizing the simulation using a geometric parameter, i.e. the degree of solvation of the buried interface, resulted in a testable prediction regarding which mutations would result in a stable dimer. We present experimental data (denaturation and binding measurements) to show that an intuitive parameter based on physical reasoning can be useful for characterizing simulations that are difficult to analyze quantitatively.

Published by Elsevier Inc.

1. Introduction

Wt streptavidin tetramer is a structural dimer of two "native" dimers, because the buried solvent accessible surface area (SASA) at the dimer interface (~1300 Å^2, or ~22% of the monomer SASA) is significantly larger than the contacts across the dimer–dimer interface (~8.1–9.6% of the monomer SASA) (Fig. 1) [1,2]. Because the streptavidin subunits are organized into monomer, dimer and tetramer, mutations at the dimer–dimer interface can disrupt the tetramer formation without directly affecting monomer folding or dimer association. Despite limited contacts, the interactions at the tetramer interface are known to be important for high affinity biotin binding. This conclusion is supported by both structural and biochemical data, which show that the residue W120 is swapped between neighboring subunits [1,2], and either mutating W120 to A, F, or K [3–6], or disrupting the tetramer association using interface mutations [7] to prevent the swapping of W120 reduces the biotin affinity from $K_d \sim 10^{-14}$ M to 10^{-8}–10^{-7} M. The residue contributes to biotin binding in several ways, for example, by directly contacting the bound ligand as well as by organizing the disordered binding loop, i.e. residues 45–50 [2]. Furthermore, tetramerization contributes to the stability of the molecule by burying hydrophobic residues at the dimer–dimer interface, including L109 and V125. As such, wt streptavidin has significantly higher stability (T_m = 75 °C) [8,9] than the dimer and the monomer, both of which easily denature and precipitate [10,11], and require various surface mutations for stabilization [7,11].

While the role of streptavidin tetramerization has been studied extensively, the significance of dimer association is usually overlooked during the structural and functional analysis of streptavidin. Although the dimer interface is not part of the ligand binding pocket, dimer formation is likely to be functionally relevant. For example, biotin binding has been shown to induce structural tightening across the dimer interface [12], suggesting a coupling between biotin binding and dimerization. Biotin also helps fold streptavidin dimer purified from bacterial inclusion body

* Corresponding author. Tel.: +1 716 645 1199; fax: +1 716 645 3822.
E-mail address: sjpark6@buffalo.edu (S. Park).

1093-3263/$ – see front matter. Published by Elsevier Inc.
doi:10.1016/j.jmgm.2010.09.009

[7]. Finally, the native dimer formation is required to assemble a functional tetramer, and thus the measured biophysical properties of streptavidin tetramer include the contributions from the native dimer. Together, these observations suggest that a complete description of the structure–function relationship in streptavidin needs to include the contributions from the dimer interface as well as the interactions at the tetramer interface.

Despite high resolution structures of streptavidin, the details of residue contacts at the dimer interface remain poorly understood [3,13]. In fact, to our knowledge, there has been no systematic study to date on how mutations at the dimer interface affect subunit association and biotin binding. To understand the structural basis of dimer association and to evaluate the effects of interfacial mutations, we used MD simulation and biochemical characterization to analyze mutations at the dimer interface. In particular, we investigated how mutations at the dimer interface affects dimer and tetramer association as well as biotin binding. In addition to elucidating the structure–function relationship at the dimer interface, correlating interfacial mutations with oligomerization also provides a strategy for modulating oligomerization through designed interfacial mutations. The native dimer interface of streptavidin consists of short polar side chains that interdigitate to form networks of hydrogen bonds and van der Waals contacts. We tested if large and small residues at the interface can be rationally redistributed in order to design other mutant interfaces that similarly form complementary surfaces. Engineered dimer mutants can serve as building blocks for constructing novel streptavidin oligomers for applications in biotechnology, and provide a lesson on remodeling the protein–protein interface by engineering the sterics.

Our study highlights an important limitation of simulated dynamics. Although simulations are used frequently during structure–function studies [14,15], an accurate energy prediction is often difficult due to significant fluctuations among the simulated structures. To this end, we show that a quantitative model based on detailed energy calculations can result in unreliable predictions when applied to non-equilibrium structures, as we see for some of our simulated mutants. To circumvent the errors due to limited sampling, we constructed a geometric solvation parameter that measures solvent penetration into the previously buried surface. Although the solvation parameter provides a heuristic description of the simulation, it summarizes the physically intuitive conclusion from the simulation, i.e. an unstable dimer will allow more solvent into the interfacial space, and leads to clear, testable predictions. Using a descriptive metric is especially useful if the simulation does not reach full equilibrium during the simulation or the simulated structures exhibit large fluctuations [16]. We confirmed the prediction that the solvation of the interface correlates with the stability of the protein by characterizing the mutants in vitro. Therefore, MD simulation can differentiate stable and unstable mutants and predict how an interfacial mutation would affect oligomer formation, if a suitable molecular descriptor based on physical reasoning can be constructed. Bridging microscopic observations with macroscopic phenomena through parameterization should be useful in extending the applications of MD to protein engineering challenges.

2. Materials and methods

2.1. Streptavidin structures

The coordinates of streptavidin were obtained from 1SWE. The four subunits are similar and have main chain rmsd of 0.4–0.53 Å from each other. For dimer simulations, we used the subunits A and B, and point mutants derived from them. Both 1SWE and other streptavidin crystal structures in PDB (e.g. 2IZL) contain several ordered water molecules at the interface. Since buried water molecules play important structural roles [17,18], we included solvent molecules from the crystal structure in the simulation if they have zero or near zero solvent accessible surface area (SASA), as computed using NACCESS [19]. To maintain a symmetry in the system, we also included seven water molecules that have small but nonzero SASA for a total of 18 water molecules in the tetramer.

All definitions of buried residues are based on the scheme described in Lo Conte et al. [20]. There are 43 (46) interfacial residues in chain A (B) that have a reduced SASA in the dimer than in the monomer. Of these, 33 (35) residues are within 0.5 Å of a non-hydrogen atom of the opposite subunit, and 8 (10) are fully buried (SASA < 1 Å^2) in the dimer. Two additional residues, L73 and W75, of chain B are considered buried at the interface according to the used selection scheme, but these are core residues of a monomer and are not genuine interface residues.

2.2. Simulation details

The MD simulations were performed using NAMD v. 2.6 [21] with Charmm 27 [15]. Streptavidin oligomers were immersed in a water box with a minimum of 12 Å separation to the wall. The net charge in the system was neutralized using NaCl to the final ionic concentration of 100 mM. Water molecules were energy minimized for 5000 steps first with the protein fixed, then the entire system was relaxed for another 5000 steps before the temperature of the system was increased to the final temperature of 310 K over 1.55 ps. The simulation was conducted under constant pressure (1 atm) and temperature (NPT ensemble) using 1 fs time steps under periodic boundary conditions. Electrostatics were treated using the particle mesh Ewald sum. All simulations were performed for a minimum of 10 ns. The trajectories were visualized and analyzed using VMD [22].

2.3. Binding free energy

The free energy of binding was computed essentially as in [23] and is summarized below:

$$\Delta G_{binding} = (\Delta E_{MM} + \Delta G_{solv}) - T\Delta S = \Delta G^{*}_{binding} - T\Delta S \tag{1}$$

$$\begin{aligned}\Delta E_{MM} &= E_{MM}(\mathrm{A:B}) - E_{MM}(\mathrm{A}) - E_{MM}(\mathrm{B})\\ &= E_{elec}(\mathrm{A:B}) + E_{vdw}(\mathrm{A:B}) + E_{conf}(\mathrm{A:B}) - E_{elec}(\mathrm{A})\\ &\quad - E_{vdw}(\mathrm{A}) - E_{conf}(\mathrm{A}) - E_{elec}(\mathrm{B}) - E_{vdw}(\mathrm{B}) - E_{conf}(\mathrm{B})\\ &= E_{elec}(\mathrm{A:B}) + E_{vdw}(\mathrm{A:B}) - E_{elec}(\mathrm{A}) - E_{vdw}(\mathrm{A})\\ &\quad - E_{elec}(\mathrm{B}) - E_{vdw}(\mathrm{B})\\ &= \Delta E_{nonb}\end{aligned} \tag{2}$$

$$\Delta G_{solv} = \Delta G_{PB} + \Delta G_{SA} \tag{3a}$$

$$\Delta G_{PB} = \Delta G_{PB}(\mathrm{A:B}) - \Delta G_{PB}(\mathrm{A}) - \Delta G_{PB}(\mathrm{B}) \tag{3b}$$

$$\begin{aligned}\Delta G_{PB}(\chi) &= G_{PB,wat}(\chi) - G_{PB,prot}(\chi) \quad \text{for } x = \mathrm{A,B, \ or \ A:B}\\ \Delta G_{SA} &= \gamma\Delta\mathrm{SASA} + b\\ \Delta\mathrm{SASA} &= \mathrm{SASA(A)} + \mathrm{SASA(B)} - \mathrm{SASA(A:B)}\end{aligned} \tag{3c}$$

For each simulated trajectory, we extracted the protein coordinates every 50 ps for a total of 200 frames. The molecular mechanics (ΔE_{MM}) energy of binding was computed using the namdenergy plugin of VMD using the dielectric constant $\varepsilon = 2$ or 4. ΔE_{MM} contains only the nonbonded energies between chain A and B, since the conformational energy contribution is cancelled exactly when using a single trajectory to obtain the conformation energies of both the complex (A:B) and the interacting subunits (A or B) (Eq.

(2)). The electrostatic contribution to the solvation energy difference ΔG_{PB} between the bound and unbound states (Eq. (3b)) was computed by calculating the solvation energy of the complex in water ($\varepsilon = 78.54$) and subtracting the solvation energy for the interacting subunits using APBS [24]. The calculation was repeated for $\varepsilon = 2$ and 4. The nonpolar solvation energy (Eq. (3c)) was assumed to be proportional to the buried solvent accessible surface area of the complex (computed using VMD) using the parameters $\gamma = 0.00542$ kcal/mol/Å^2 and $b = 0.92$ kcal/mol [25]. The solute entropy term ($T\Delta S$) was not calculated since it is difficult to estimate accurately and should be similar for wt and mutant structures. We report $\Delta G^*_{binding}$ as the free energy of binding.

The local nonbonded interaction energy ($\Delta E_{MM,local}$) was computed similarly, except the summation was limited to the atoms that are within 4, 6, 8, or 10 Å of residues 74 and 76 of either chain. The selection was updated for each frame and the dielectric constant was set to 1, 2, or 4. The interaction energy with Wat206 was added if the water is within the distance cutoff. For both free energy and local interaction energy calculations, we report the standard deviation rather than the error of the mean since the individual frames do not constitute independent measurements.

2.4. Solvation of buried interface

The solvation of the buried interface was parameterized by counting the water molecules that are within 4 Å of the residues 74, 76, and 91 of chain A and B as a function of the simulation time. Alternatively, we computed the SASA of eight interfacial residues that have zero SASA (residues 58, 72, 74, 76, 89, 91, 93, and 111) using NACCESS to parameterize dimer dissociation.

2.5. Plasmid and constructs

To construct a bacterial expression vector for wt streptavidin, we PCR amplified the residues 1–139 of the mature form of wt streptavidin using the primers 5′-GCATACGTGCTAGCGACCCCTCCAAGGACTCGAAG-3′ and 5′-GCATACGTGGATCCGGAGGCGGCGGACGGCTTCAC-3′ and ligated the resulting fragment with a bacterial expression vector pBE1 (derived from pRSET-A) using NheI and BamHI. The resulting pBE1-wtSA contains a gene with a C-terminal FLAG tag (DYKDDDDK) for detection and an N-terminal 6xHis tag for affinity purification.

The mutants vectors for AA, GV, TG, and LG were constructed by cassette mutagenesis using the following mutagenic primers:

- AA: 5′-GACGGCAGCGGCACCGCCCTCGCCTGGGCCGTGGCCTGGAAGAATAACTAC-3′
- GV: 5′-AGCGGCACCGCCCTCGGCTGGGTCGTGGCCTGGAAGAATAACTAC-3′
- TG: 5′-GACGGCAGCGGCACCGCCCTCACGTGGGGTGTGGCCTGGAAGAATAACTAC-3′
- LG: 5′-GACGGCAGCGGCACCGCCCTCCTGTGGGGCGTGGCCTGGAAGAATAACTAC-3′.

All constructs were confirmed by sequencing.

2.6. Protein expression and purification

Wt and mutant streptavidin were expressed and purified from bacteria using a protocol modified from Howarth et al. [26]. We transformed *E. coli* BL21 (DE3) with wt or mutant plasmids and selected the transformants on LB plates containing 100 μg/ml ampicillin. Overnight 3 ml LB cultures were started from 4 to 6 colonies and diluted 100-fold in the morning. The cultures were induced at $OD_{600} = 0.9$ with 100 μg/ml isopropyl β-D-thiogalactopyranoside (Sigma) for 4 h at 37 °C, after which the cells were harvested and resuspended in 4 ml B-PER (Pierce), vortexed for 1 min, and centrifuged at 14,000 rpm for 20 min. The pellet was suspended in 4 ml B-PER with 40 μg/ml lysozyme (Sigma) and incubated at 20 °C for 5 min. 17 ml inclusion wash buffer (WB1, 50 mM Tris–HCl pH 8.0, 100 mM NaCl, 0.5% Triton X-100) was added to the suspension and vortexed until the solution became homogeneous, and the mixture was spun at 14,000 rpm. The pellet containing the inclusion body was washed twice in WB1 and was dissolved in 1 ml 6 M guanidine hydrochloride (GuHCl, Sigma) at pH 1.5. The insoluble fraction was removed by centrifugation and the supernatant was added drop by drop to 40 ml PBS pH 7.4 under rapid stirring at 4 °C to refold the protein. The solution was kept stirring at 4 °C overnight, after which the precipitates were removed by centrifugation. The refolded protein was concentrated to 2 ml using Amicon Ultra centrifugal filters (Millipore) with 10 kDa cutoff and mixed with 250 μl TALON metal affinity resin (Clontech) for 6xHis affinity purification. After 1 h incubation at 20 °C with occasional stirring, the resin was washed in 10 ml resin wash buffer (WB2, 150 mM NaCl, 50 mM Tris–HCl pH 7.0, 50 mM imidazole) twice, and eluted in 3× 1 ml elution buffer (EB, 150 mM NaCl, 50 mM Tris–HCl pH 7.0, 200 mM imidazole). The positive fractions were combined and concentrated to ∼50 μl. The purified protein solution was analyzed on 10% SDS-PAGE gel with or without boiling, with or without biotin dimer (Pierce).

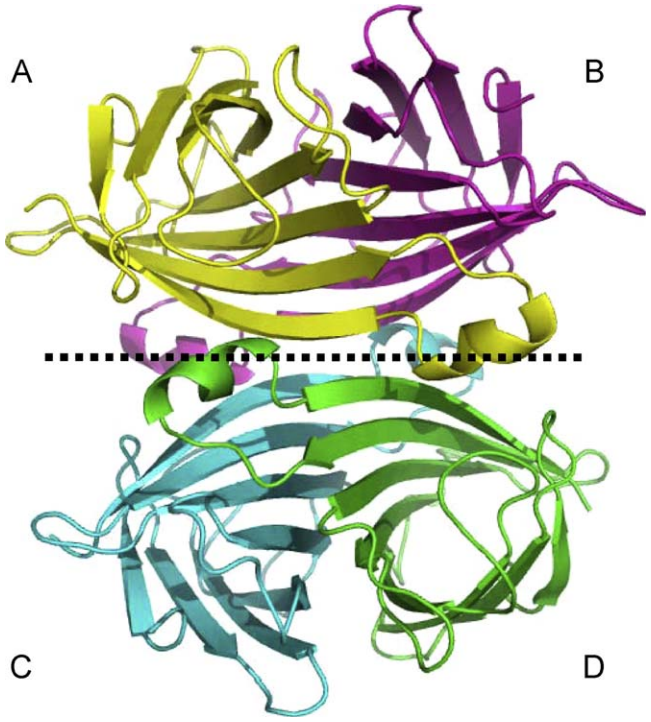

Fig. 1. A streptavidin tetramer consists of two native dimers. The dimer–dimer interface is indicated as a dashed line. Figures were generated using Pymol (DeLano Scientific).

2.7. Circular dichroism spectroscopy

The circular dichroism spectra were obtained on J-815 CD spectropolarimeter with a temperature controller using a cuvette with 1 mm pathlength. A spectral bandwidth of 1 nm was used for data collection. Streptavidin was prepared in PBS (pH 7.4) at the concentration of 2.5 μM. To induce heat denaturation, the temperature was raised from 20 to 95 °C, while measuring the CD spectrum between 200 and 250 nm for every 1 °C increment. The fraction

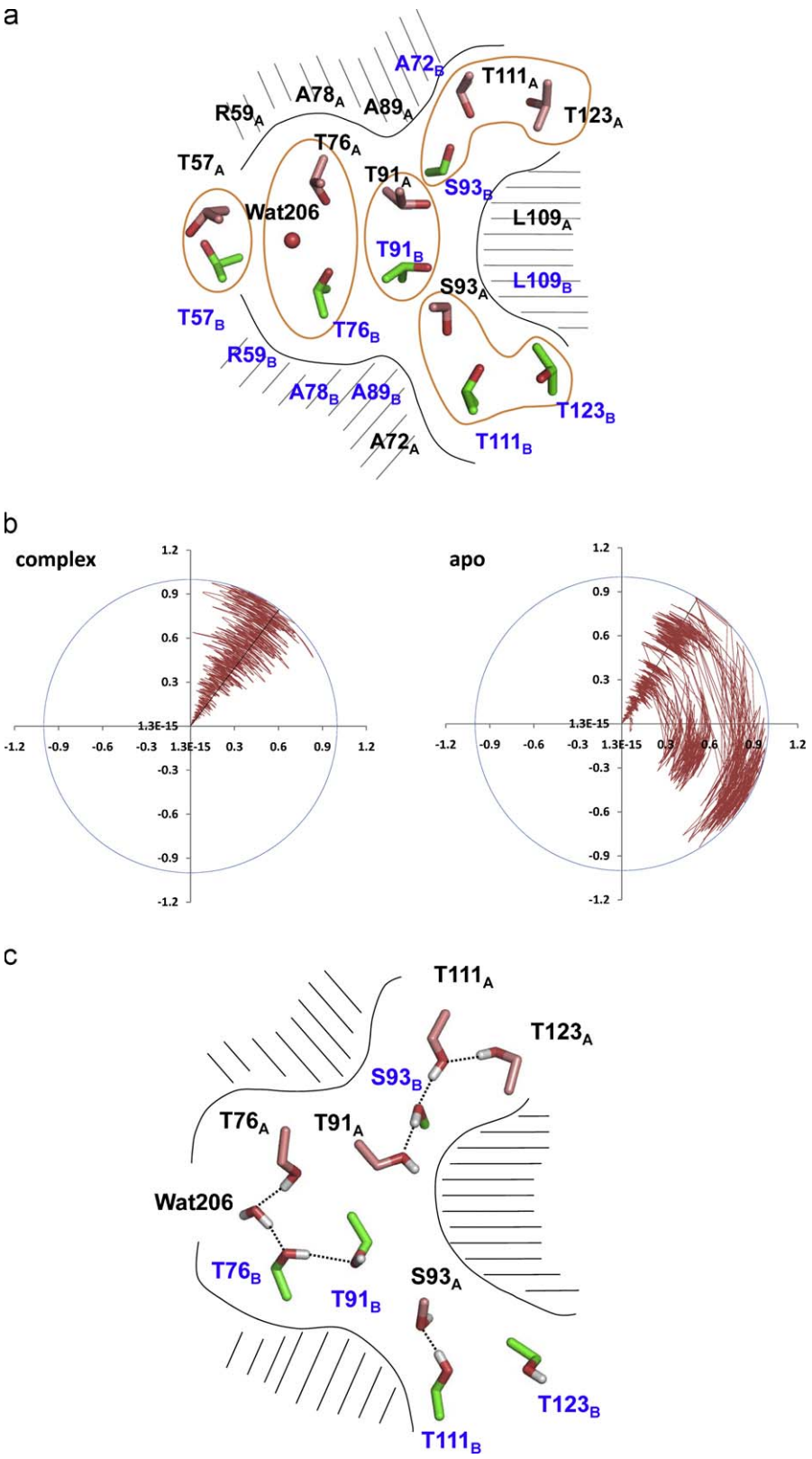

Fig. 2. (a) The arrangement of interface side chains in the crystal structure 1SWE. The polar residues and Wat206 form clusters of intermolecular hydrogen bonds (orange circles). Hydrophobic residues and atoms surround the polar residues and form a barrier to keep the solvent molecules from entering the buried interface (hatched). The amino acid side chains are shown as sticks with chain A residues in pink and chain B residues in green. The chain number is shown as a subscript following the residue number. (b) Streptavidin tetramer was simulated either with or without bound biotin. All four T91 side chains of the biotin–streptavidin complex remain as in the crystal structure, whereas two in the apo structure (one in each native dimer) rotate to different rotamers. The T91 $\chi 1$ dihedral angle was computed and plotted from the *x*-axis, with the simulation time increasing along the radius. The straight line corresponds to the conformation in the crystal structure (1SWE). The biotin force fields used in the simulation were provided by T. Lazaridis. (c) As a result of the T91 side chain rotation, the hydrogen bonding network at the interface is significantly different in the apo structure. The rotation of Wat206 results in a loss of one water hydrogen bond. The main chain of T57 oxygen is omitted for clarity. Compare with Fig. S1 which shows Wat206 in the complex structure.

of denatured protein f was fitted to the integrated form of the van't Hoff equation [4],

$$f = \frac{1}{1 + (1/\exp(\Delta H_{vH}/R(1/T_m - 1/T)))} \quad (4)$$

where ΔH_{vH} is the transition enthalpy and T_m is the melting temperature. The Matlab curve fitting toolbox (The MathWorks, Inc.) was used to fit the data and find T_m.

Because the fit to Eq. (4) was not sensitive to the precise value of ΔH_{vH}, the enthalpy at the melting temperature was computed instead by fitting the data near the transition temperature by linear regression to Eqs. (5a) and (5b). The fitted enthalpy and entropy values are reported in Table 3.

$$dG = aT + b \quad (5a)$$

$$dG_{T_m} = dH_{T_m} - T_m dST_m = 0 \quad (5b)$$

The free energy difference at $T = 69\,^{\circ}C$ (average T_m of wt and mutant streptavidin) was computed using the Gibbs–Helmholtz equation:

$$\Delta G(T) = \Delta H_{T_m}\left(1 - \frac{T}{T_m}\right) - \Delta C_p\left(T_m - T + T\ln\left(\frac{T}{T_m}\right)\right) \quad (6)$$

The difference in heat capacity between the folded and unfolded state, ΔC_p, of a protein with N residues is approximated using $\Delta C_p = -172 + 17.6\,N$ (cal/mol) [27,28].

2.8. Affinity measurement

The dissociation constant (K_d) was measured by fluorescence quenching using biotin-4-fluorescein (B4F) (AnaSpec). Purified protein was quantified by UV and a titrating amount of the protein was mixed with 0.16 nM B4F in 200 μl PBS pH 7.4 with 0.01% BSA (PBSA). After 1 h incubation at 37 °C, the florescence intensity was measured on a microplate reader (Synergy 4, BioTek instruments, Inc.). The fraction of bound B4F was determined based on the degree of fluorescence quenching, as described [29,30].

2.9. Flow cytometric analysis of biotin binding

The purified protein was quantified by UV using the extinction coefficient 4182 $M^{-1}\,cm^{-1}$. To test for biotin binding, equal amounts of the purified proteins were mixed with 50 μl of biotin coated microspheres (Bangs Laboratories) that have been pre-equilibrated in PBSF (PBS pH 7.4 with 0.1% BSA), and incubated for 1 h at RT. The beads were then washed in 500 μl of PBSF twice and re-suspended in 50 μl PBSF. To quantify the proteins on the beads, we incubated the beads with 1 μl of monoclonal mouse anti-FLAG antibody M2 (Stratagene) for 30 min at RT, followed by 30 min labeling with fluorescein isothiocyanate (FITC) conjugated goat anti-mouse IgG antibody (Sigma). To determine if the bound protein has one or multiple biotin binding sites, we first labeled the protein immobilized on the beads with biotinylated rabbit anti-TNF antibody (BD Biosciences), and then used FITC-conjugated goat anti-rabbit IgG antibody for visualization (Sigma). The labeled microspheres were analyzed on a Quanta MPL flow cytometer (Beckman Coulter).

3. Results

3.1. Molecular dynamic simulations of streptavidin tetramer and dimer

The streptavidin dimer interface contains a central hot spot consisting of hydrophilic residues surrounded by a ring of hydrophobic residues (Fig. 2a). Although the clustering of these interfacial

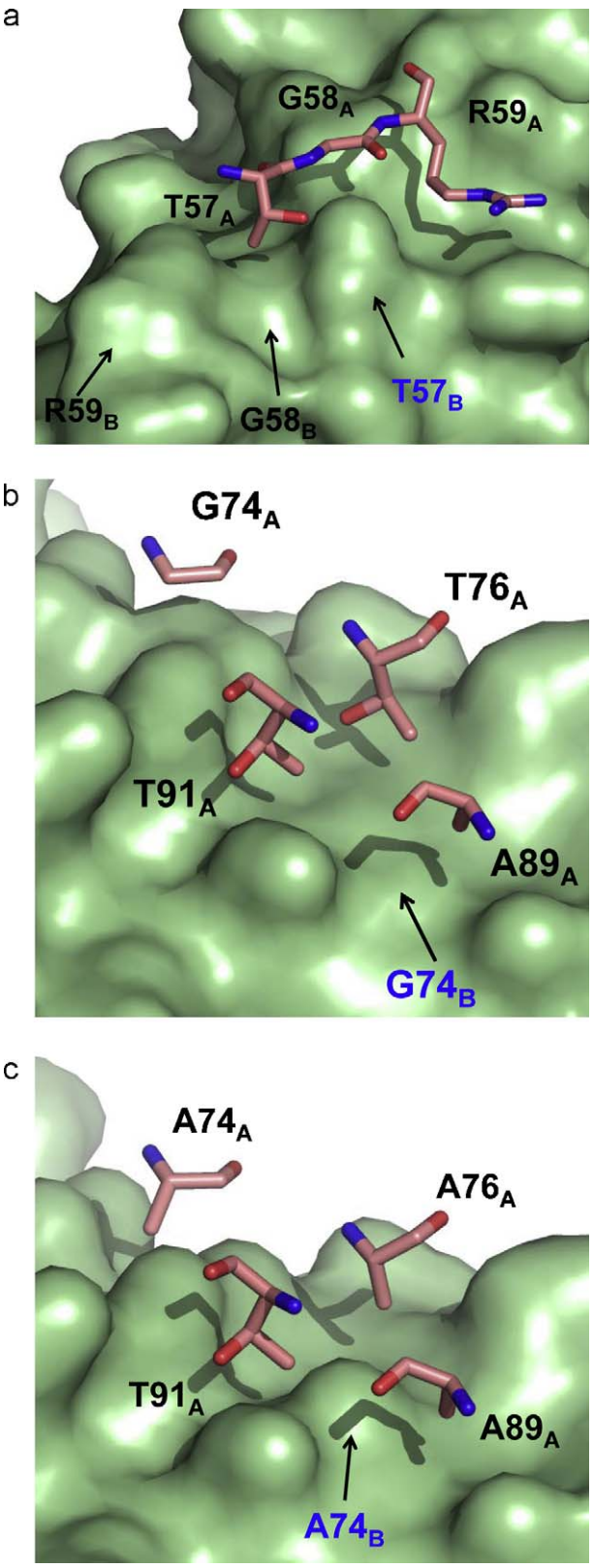

Fig. 3. (a) A knob-into-hole interaction at the interface involving T57, G58, and R59. The side chain of T57 from one chain is inserted into the groove formed by G58 of the other chain. (b) A large basin is created over G74 of one chain (arrow) which is filled by the side chains of complementing residues T76, A89, and T91 of the other chain. (c) A modeled structure of AA dimer containing G74A and T76A mutations. The mutations redistribute the side chain volume between 74 and 76 while preserving the total side chain volume.

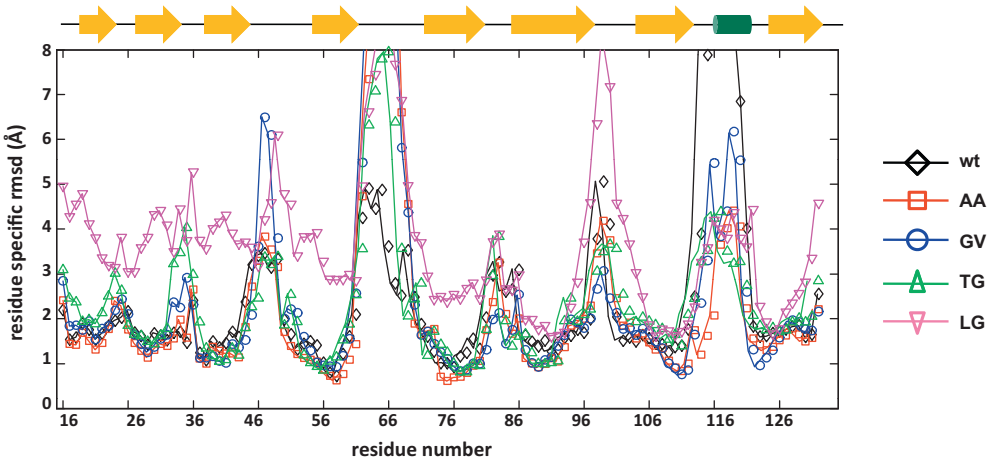

Fig. 4. Residue specific main chain rmsd for chain B residues was computed by superimposing the simulated structures to the initial structure using chain A main chain atoms. Wt and three mutants (AA, GV, and TG) have comparable rmsd values for all nonloop residues, whereas they are larger for some LG residues. Wt (black, diamond), AA (red, square), GV (blue, circle), TG (green, up arrow), and LG (magenta, down arrow). The secondary structures are indicated above the figure.

residues is suggestive of the "O" ring model of the protein interaction interface [31], the distribution of polar and nonpolar groups is opposite of the more typical hot spot that contains a hydrophobic center and a hydrophilic ring [32,33]. Buried polar residues are energetically unfavorable unless they form hydrogen bonds [34], but buried hydrogen bonds can also contribute to stability [35,36], because they are on average ~1.2 kcal/mol stronger than solvent exposed hydrogen bonds [37]. In this regard, the hydrogen bonding network at the dimer interface may play an important role in stabilizing the complex. To study the side chain dynamics at the dimer interface, we simulated the biotin-bound streptavidin tetramer (1SWE) and examined the hydrogen bonds among buried residues. The hydrogen bonds present in the crystal structure are stable and specific, since they are maintained throughout the simulation (Fig. S1). However, the simulation of apo-streptavidin shows that the side chain of buried T91 readily rotates to a different rotamer state to form new hydrogen bonds not seen in the crystal structure (Fig. 2b and c), suggesting the interface is much more dynamic in the apo structure. In both apo and complex structures, one buried water molecule in each dimer, Wat206 of the dimer A/B and Wat201 of dimer C/D, forms stable hydrogen bonds with T57 main chain oxygens (two acceptors) and T76 side chain hydroxyls (two donors). The stability of these hydrogen bonds suggests that the buried water molecules play important structural roles [17,18] (Table S1). In the simulated apo structures, Wat206/Wat201 rotates from the initial structure in order to donate two hydrogen bonds to T57 and T76, while accepting one hydrogen bond from the remaining T76 (Fig. 2c). Therefore, biotin binding also induces structural differences at the interface involving protein–water interactions.

Reducing the simulated system size while ensuring relevant interactions are correctly accounted for has a practical importance by reducing the complexity of calculation. We repeated the apo simulation with only a dimer and compared the results with the tetramer. By simulating a dimer, we are assuming that the dynamics at large and small scales are only weakly coupled. This is a reasonable assumption since it is the cornerstone of the coarse graining method, which is commonly used to simulate large systems [38–40]. Both non-loop residue rmsd values (1.0 Å of tetramer vs. 1.1 Å of dimer) and buried hydrogen bonds are nearly identical in dimer and tetramer simulations. The protein interactions with Wat206 and Wat201 are similarly conserved (Fig. S2). Since simulating a native dimer reproduces all major interactions at the interface as simulating the full tetramer (Table S1) while reducing the system size by ~45%, we decided to include only a dimer in our subsequent simulations.

3.2. Complementary pairs at the interface

The dimer interface is stabilized by both hydrogen bonds and van der Waals contacts, including several "knob-into-hole" type interactions [41]. Knob and hole interactions are used in naturally occurring and designed proteins to increase the stability and specificity of interaction [42–44]. Because steric complementarity is important for specificity, introducing correlated mutations at the interface through a knob and hole design can be a convenient method to modulate subunit association. There are several residues at the dimer interface that exhibit extensive surface complementarity, including (i) T57, G58, R59 (Fig. 3a) and (ii) G74, T76, A89, and T91 (Fig. 3b). We introduced targeted mutations at G74 and T76 to test how well surface complementarity can be designed. These residue positions were selected because they are fully buried at the interface, and therefore, steric requirements are likely to be more stringent at these positions compared to solvent exposed positions, e.g. T57 and G58, leading to a more rigorous test of our design. First, we mutated both residues to Ala (i.e. G74A and T76A, abbreviated here as AA) to replace a side chain–main chain interaction in wt with a side chain–side chain hydrophobic interaction in the mutant (Fig. 3c). The substitutions change the polarity of the interaction from hydrophilic to hydrophobic but conserves the combined side chain volume. Therefore, the mutations should introduce minimal steric perturbation [45]. We simulated AA to characterize how the mutations affect the interactions at the interface. The simulated interfaces of wt and AA are similar, except Wat206 in AA now hydrogen bonds to T57 main chain oxygens only (Fig. S3).

We constructed and simulated other combinations of mutation, including GV, TG, and LG, to explore other side chain arrangements at the interface. GV replaces a side chain hydroxyl with a methyl, resulting in a modest increase in volume (~20–25 $Å^3$). Modeling TG and LG into wt backbone showed that the side chains of T74 and L74 may complement the new hole that is created at G76. Therefore, all three mutants may be equally stable. Alternatively, the swapping of knob and hole residues in TG and LG may destabilize the mutant structures by causing mismatched side chain packing. Our goal was to use MD simulation to model the effects of these mutations by simulating various ways the side chains may interact, and use the simulation to predict if the designed mutant can form a stable oligomer. A global analysis, such as the main chain rmsd, was

Table 1
The free energy of dimer association $\Delta G^*_{binding}$ (kcal/mol) was computed using two tion between 5 and 10 ns of simulation were used to compute the energy. The numbers in parentheses are standard deviations. The numbers in bold were used to plot Fig. 5a.

	ΔE_{MM}	ΔG_{PB}	ΔG_{SA}	$\Delta G^*_{binding}$
$\varepsilon = 2$				
Wt	−269.8 (13.6)	216.8 (12.3)	17.3 (0.3)	**−70.3 (18.4)**
AA	−243.6 (14.8)	187.0 (13.4)	16.5 (0.7)	**−73.2 (20.0)**
GV	−261.7 (21.6)	184.3 (13.3)	16.2 (0.7)	**−93.6 (25.4)**
TG	−234.3 (19.0)	170.2 (16.4)	16.7 (0.6)	**−80.8 (25.1)**
LG	−291.5 (15.0)	215.8 (11.1)	17.2 (0.4)	**−92.9 (18.7)**
$\varepsilon = 4$				
Wt	−198.7 (8.0)	104.5 (5.8)	17.3 (0.3)	−111.4 (9.9)
AA	−181.1 (10.3)	90.6 (6.4)	16.5 (0.7)	−107.0 (12.2)
GV	−193.5 (13.5)	89.1 (6.3)	16.2 (0.7)	−120.5 (15.0)
TG	−171.2 (11.8)	82.8 (7.9)	16.7 (0.6)	−105.1 (14.2)
LG	−205.0 (9.0)	104.4 (5.4)	17.2 (0.4)	−117.8 (10.5)

not informative in this regard, since all sequences had similar values (Fig. S4). However, if the structures are superposed using chain A residues, the residue specific rmsd of chain B was significantly larger for some LG residues (Fig. 4). The rmsd values are larger for the residues in the first half of the protein because they are located farther from the dimer interface and the disruption of the interface causes larger displacements for these distant residues from their respective initial positions.

3.3. Computed free and internal energy

The contribution from a residue to the binding energy can be estimated by computational alanine scanning [25]. Alanine mutants are straightforward to model because they usually adopt similar global structures as wt. However, the substitutions that increase the side chain volume are more difficult to model since they can induce large structural changes including backbone adjustments. In this regard, there have been attempts to incorporate backbone flexibility in side chain modeling [46]. We tested if the free energy of binding for the designed streptavidin mutants can be computed based on simulated structures [47] in order to make a quantitative prediction of their dimer stability (Fig. 5a). The free energy was calculated by adding the molecular mechanics interaction energy in a homogeneous dielectric medium of $\varepsilon = 2$ or 4 with the solvation energy term computed by solving the Poisson Boltzmann model of solvation with APBS [24]. The computed molecular interaction energy term includes large electrostatic contributions from surface residues, including D61, K80, R103, E116 that form stochastic salt bridges during the simulation. Because the electrostatic contributions are weighted more heavily when using a smaller value of the dielectric constant, the predictions resulting from different values of ε can be qualitatively different (Table 1). For both values of ε, however, the simulated free energy of binding fluctuates significantly and results in overlapping ranges of computed energy for wt and mutants, making it difficult to predict their relative stability with high confidence. The observed fluctuations are not errors caused by simulating dimers instead of tetramers, since computing the free energy using the tetramer structures results in similar values of computed energy and standard deviation (data not shown).

Because the fluctuations to the computed energy are caused by interactions involving distant loop residues, we reasoned that including only the interactions that are local to the mutational site may yield more stable results. To this end, we calculated the interaction energy (sum of nonbonded and conformational energies) locally around the mutated residues 74 and 76. Modeling the effects of a mutation locally is equivalent to assuming that these mutations do not cause global structural changes, which is implicitly assumed

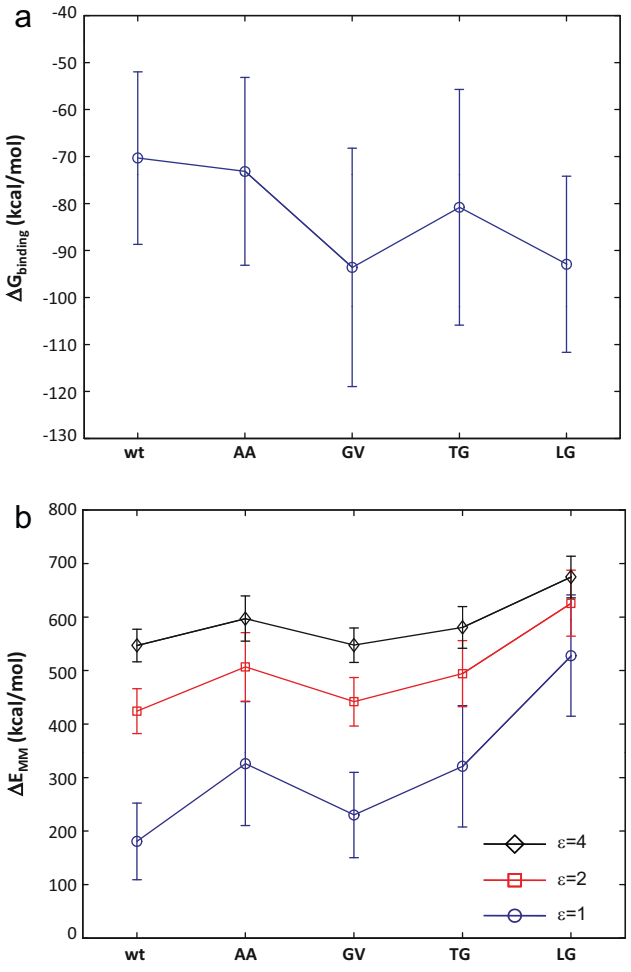

Fig. 5. (a) The free energy of binding $\Delta G^*_{binding}$ for dimerization was computed from the simulated trajectories by adding the molecular mechanics interaction energy and solvation energy. The average and error bars (standard deviation) were computed using the structures between 5 and 10 ns for each simulation. A dielectric constant of 2 was used for the interior of the solute during the solvation energy calculation. (b) The interaction energy (sum of nonbonded and conformational energy) for the residues within 8 Å of residues 74 and 76 for $\varepsilon = 1$, 2, or 4. Increasing the dielectric constant reduces the contribution from favorable nonbonded electrostatic interaction and thus increases the total interaction energy.

in most homology models. We defined spheres of radius 4, 6, 8, or 10 Å around the mutated residues and computed the local interaction energy $\Delta E_{MM,local}$ by including only those atoms that are within the sphere (Table 2). Wat206 was also included in the calculation but bulk water molecules were not included. We repeated the energy calculation using $\varepsilon = 1$, 2, or 4. The computed energy values show that all mutations are destabilizing but the increase in the potential energy was the largest for LG (Fig. 5b). Even when the energy calculation is limited to local interactions, it is still difficult to determine if the mutants are qualitatively different from wt and from each other due to large uncertainties in the computed energy.

3.4. Solvation of the buried interface

Energy calculation depends sensitively on the structure since computed energy depends on atomic coordinates. In particular, if a simulation does not reach an equilibrium, the energy calculation may yield qualitatively misleading stability estimates. In fact, experiments clearly show that some of the simulations do not reach an equilibrium within 10 ns (see below). It is not clear what com-

Table 2
The local molecular mechanics interaction energy $\Delta E_{MM,local}$ (kcal/mol) including either nonbonded interactions only or both nonbonded and conformational energies were computed using different distance cutoff values. The standard deviations are included in parentheses. The values in bold were used to plot Fig. 5b.

	$\Delta E_{M,M,local}$ (nonbonded)			
	4 Å	6 Å	8 Å	10 Å
$\varepsilon = 1$				
Wt	63.7 (43.8)	−97.6 (56.7)	−678.6 (69.1)	−844.7 (100.4)
AA	188.3 (59.7)	−90.7 (54.6)	−543.0 (114.9)	−886.7 (94.3)
GV	134.2 (41.0)	−8.7 (49.2)	−621.2 (78.4)	−759.0 (122.6)
TG	99.6 (48.0)	−114.6 (52.3)	−520.0 (114.1)	−830.7 (106.3)
LG	154.0 (55.2)	−84.7 (53.8)	−381.7 (140.4)	−783.3 (91.6)
$\varepsilon = 2$				
Wt	7.1 (22.5)	−104.9 (29.1)	−439.9 (35.9)	−571.0 (50.3)
AA	69.7 (30.3)	−103.6 (28.6)	−373.4 (59.2)	−593.5 (49.2)
GV	41.8 (21.2)	−61.6 (24.7)	−410.4 (39.7)	−523.8 (61.9)
TG	28.7 (24.4)	−109.1 (26.8)	−354.8 (58.3)	−547.4 (54.1)
LG	49.2 (27.7)	−98.6 (27.9)	−290.1 (70.7)	−538.3 (48.3)
$\varepsilon = 4$				
Wt	−21.2 (12.4)	−107.8 (16.1)	−319.8 (20.5)	−433.4 (26.7)
AA	10.4 (15.9)	−110.1 (16.6)	−288.7 (32.2)	−446.8 (28.2)
GV	−4.5 (11.6)	−88.0 (13.3)	−305.0 (21.5)	−406.1 (32.7)
TG	−6.8 (13.1)	−106.4 (15.0)	−272.2 (31.2)	−405.7 (29.3)
LG	−3.2 (14.5)	−105.6 (16.1)	−244.2 (36.8)	−415.9 (28.2)
	$\Delta E_{M,M,local}$ (nonbonded + conformational)			
	4 Å	6 Å	8 Å	10 Å
$\varepsilon = 1$				
Wt	344.6 (47.1)	439.2 (57.7)	**189.1 (71.9)**	516.4 (98.8)
AA	467.0 (62.6)	470.6 (61.8)	**347.7 (116.8)**	487.1 (94.3)
GV	407.3 (41.5)	523.2 (52.7)	**232.5 (81.6)**	603.4 (123.3)
TG	375.5 (50.6)	406.1 (55.1)	**338.3 (117.6)**	495.3 (109.5)
LG	460.2 (59.1)	481.4 (54.2)	**536.9 (144.5)**	630.0 (93.9)
$\varepsilon = 2$				
Wt	288.0 (27.5)	431.9 (32.2)	**427.8 (42.1)**	790.0 (53.2)
AA	348.4 (34.7)	457.7 (38.3)	**517.3 (63.7)**	780.3 (52.6)
GV	314.8 (23.3)	470.3 (30.3)	**443.3 (46.1)**	838.6 (65.6)
TG	304.6 (28.4)	411.6 (31.7)	**503.5 (63.9)**	778.6 (60.2)
LG	355.4 (32.7)	467.5 (30.9)	**628.5 (76.6)**	874.9 (53.9)
$\varepsilon = 4$				
Wt	259.7 (19.3)	429.0 (22.0)	**547.9 (30.9)**	927.6 (36.2)
AA	289.1 (22.6)	451.2 (28.7)	**602.0 (40.7)**	927.0 (36.4)
GV	268.5 (16.0)	443.9 (21.4)	**548.7 (32.2)**	956.2 (41.2)
TG	269.1 (18.8)	414.3 (22.3)	**586.1 (39.8)**	920.3 (39.6)
LG	303.0 (21.0)	460.6 (22.4)	**674.4 (45.7)**	997.4 (38.1)

puted interaction energy means if the modeled structures do not correspond to the equilibrium structures. We therefore searched for a way to estimate the stability of the dimers without explicitly computing the interaction energy or even without requiring that the simulation reaches an equilibrium. We hypothesized that the structural changes caused by destabilizing mutations may be qualitatively different from the structural changes observed with stabilizing mutations, and these differences may become apparent early in the simulation. We compared the trajectories to one another and to wt, which is the only construct with known biochemical properties, in order to identify such structural differences. For one, we tested if the simulated structures can be parameterized by modeling the two subunits as rigid cylinders that translate and rotate around each other as rigid bodies. However, the analysis lacked a sensitivity and did not reveal a significant difference between wt and mutants (data not shown). In contrast, when we compared the protein–water interactions at the interface, there were variations in the extent of solvation between wt and the mutants. For example, the computed SASA of buried interfacial residues increased significantly for TG and LG, whereas it remained small for wt, AA, and GV (Fig. 6a). Another simple way to visualize this is by counting the number of solvent molecules near buried residues 74, 76, and 93, which rapidly increases for simulated TG and LG structures but remains low for the other three constructs (Fig. S5). Since the dissociation of an unstable complex exposes the buried surface to the bulk solvent, increased solvation may indicate the beginning of dimer dissociation. The analysis, therefore, suggests that TG and LG dimers would be less stable than wt, AA or GV.

3.5. Stability and function of wt and mutant streptavidin

To determine how well the simulation predicts the stability of the mutants, we purified wt and mutant streptavidin from bacteria and analyzed their structure and function in vitro. An SDS-PAGE analysis [4] shows wt, AA and GV are tetramers and can bind biotin to form heat resistant complexes (Fig. 7a and Fig. S6). In contrast, TG partitions between tetramer and monomer, indicating the mutant dimer is partially destabilized with respect to wt. By this assay, LG does not form a tetramer either with or without biotin. Next, we analyzed the stability of the proteins by measuring their melting temperature T_m by circular dichroism (CD) (Fig. 7b). All proteins except LG were stably folded at 20 °C, with a minimum at $\lambda = 216$ nm that is characteristic of a β sheet [48]. Based on the measured CD spectrum, LG did not appear to be folded, which may have caused high molecular weight aggregates seen on the gel (Fig. 7a, lanes LG 1 and 2). We measured the melting temperatures of the other four proteins by plotting the values at either 216 nm (wt, AA, or GV) or 232 nm (TG), and fitting them to the integrated form of the van't Hoff equation [49] (Fig. 7c). The measured stability of GV ($T_m = 76.9$ °C) is slightly higher than that of wt (75.0 °C) but

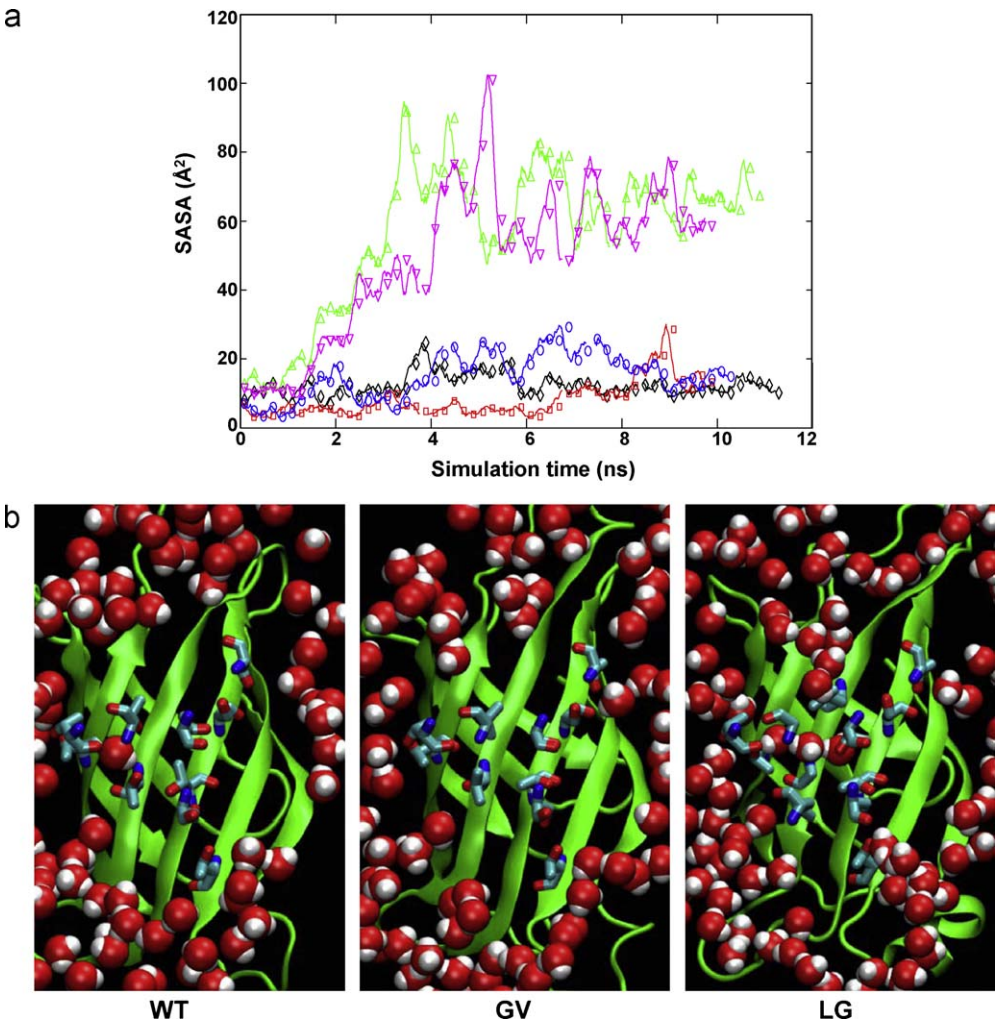

Fig. 6. (a) Computed solvent accessible surface area around buried interfacial residues shows an increase in solvation for TG and LG. In contrast, the interface of wt, AA, and GV dimer remains shielded from the bulk solvent. The notation is the same as in Fig. 4. (b) Snapshots of wt, GV, and LG interfaces showing the solvent molecules between the subunits at the end of simulation. There is a significant penetration of solvent molecules into the LG interface. Only the side chains of the buried residues are shown for clarity.

AA (67.4 °C) and TG (56.2 °C) were less stable than wt (Table 3). The large decrease in TG stability suggests that the two residue positions, 74 and 76, are not symmetric with respect to each other and simply switching the two residues results in reduced surface complementarity. The loss of water hydrogen bonds in AA and TG may have also contributed to their reduced stability.

We tested if the purified proteins are functional by measuring their affinity for biotin in a fluorescence quenching assay. We used biotin-4-fluorescein (B4F), which was previously used in a binding study [10]. The molecule is useful for characterizing functional streptavidin because its fluorescence at $\lambda = 520$ nm is quenched ~88% by streptavidin binding [29,50]. We titrated the amount of protein to obtain a quenching curve and computed the binding constant K_d by fitting the measured fluorescence intensity F between the maximum and minimum (F_{max} and F_{min}) to the quadratic binding equation:

$$f = \frac{F_{\max} - F}{F_{\max} - F_{\min}} = \frac{x - \sqrt{x^2 - 4P_0L_0}}{2L_0} \quad (7)$$

where $x = P_0 + L_0 + K_d$; P_0 = total concentration of protein; and L_0 = total concentration of B4F.

The measured binding affinities were similar and ranged from K_d = 29–49 pM (Fig. 8a). These values are higher than the wt affinity for biotin (~4×10^{-14} M from Ref. [51]) but the difference in K_d for biotin and B4F is likely caused by the proximity of the fluorophore to biotin, which must affect the intermolecular interaction. In this regard, the previously reported K_d of wt streptavidin for B4F was 140 pM [10], which is within 4 folds of our measured value.

We also tested the ability of the purified proteins to interact with biotinylated microbeads, since such binding can be analyzed using flow cytometry. We mixed purified proteins with biotin beads and fluorescently labeled the bound proteins using anti-FLAG antibody and secondary antibody, and quantified the amount of fluorescence by flow cytometry. All constructs bound biotin, including LG (Fig. 8b). The presence of LG on biotin beads was unexpected given its CD spectrum, which suggests a lack of structure, but may indicate that the protein can fold in the presence of biotin. This interpretation is reasonable because biotin is a known chaperone of streptavidin and is used to fold unstable streptavidin mutants [7].

Table 3
The denaturation temperature T_m and thermodynamic parameters used to fit the denaturation curves. The difference in the folding free energy $\Delta\Delta G$ corresponds to $\Delta G_{\text{mutant}} - \Delta G_{\text{wt}}$ at 69 °C.

	T_m (°C)	ΔH_{Tm} (kcal/mol)	ΔS_{Tm} (cal/mol/K)	$\Delta\Delta G$ (kcal/mol)
WT	75.0	−133.1	−382.3	0.0
GV	76.9	−116.2	−332.1	−0.8
AA	67.4	−90.4	−265.5	3.3
TG	56.2	−126.4	−383.9	5.0

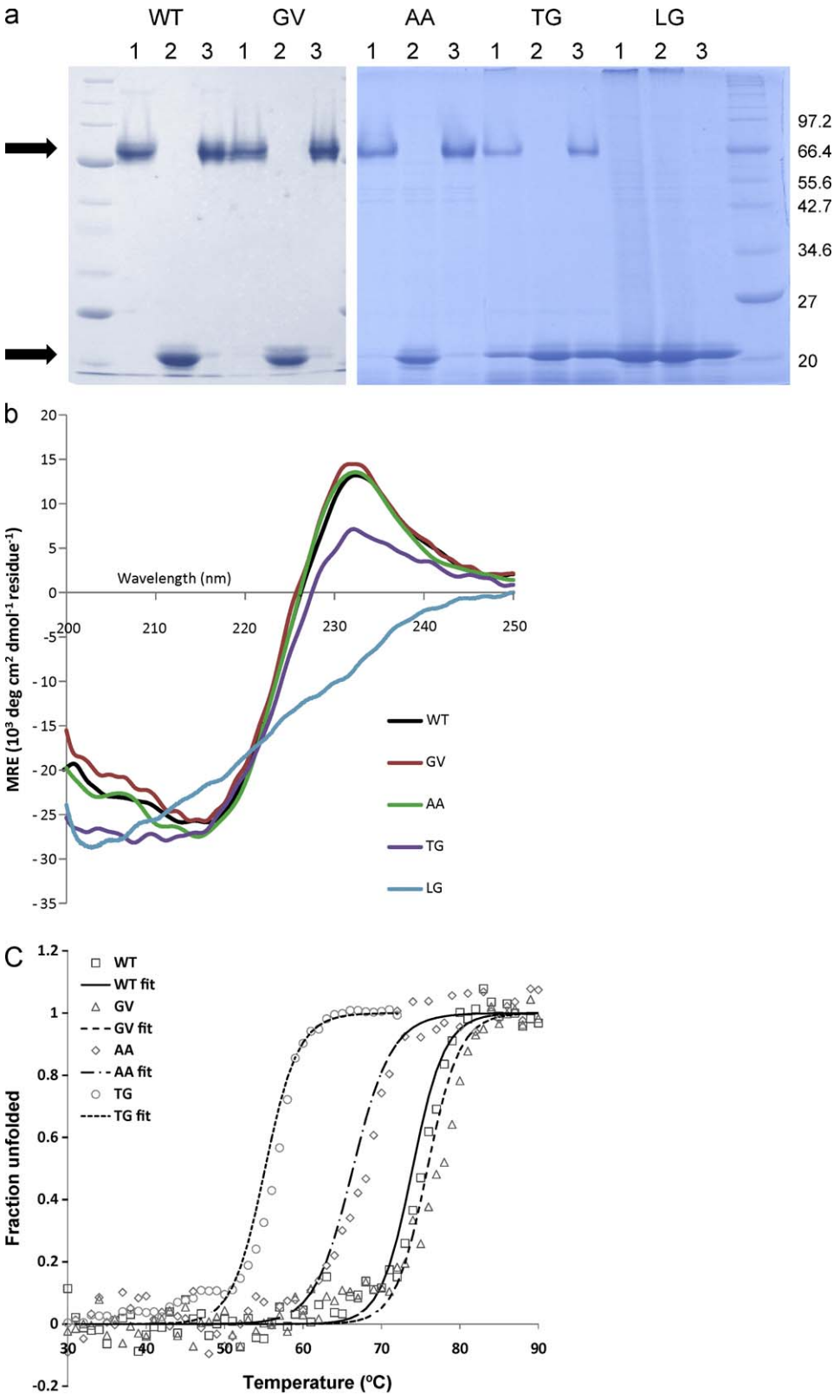

Fig. 7. (a) Purified wt and mutant streptavidin were tested for tetramer formation and biotin binding by SDS-PAGE. Each sample was loaded without boiling (1), after boiling (2), and after boiling in the presence of 2.5-fold excess amount of biotin dimer (3). Wt, GV, and AA each forms a stable tetramer and binds biotin to form a heat resistant complex. TG and LG partition into monomer and tetramer even in the presence of biotin. The upper and lower arrows correspond to the tetramer and monomer bands. The high molecular weight band of LG may correspond to nonspecific aggregates of unfolded LG, which disappears when biotin is added to the sample. (b) The mean residue ellipticity of purified wt and mutants. In addition to a broad minimum around 216 nm, all spectra, except that of LG, have a positive peak around 232 nm, which is indicative of a poly(Pro)II helix. (c) The denaturation curve for wt and mutant streptavidin.

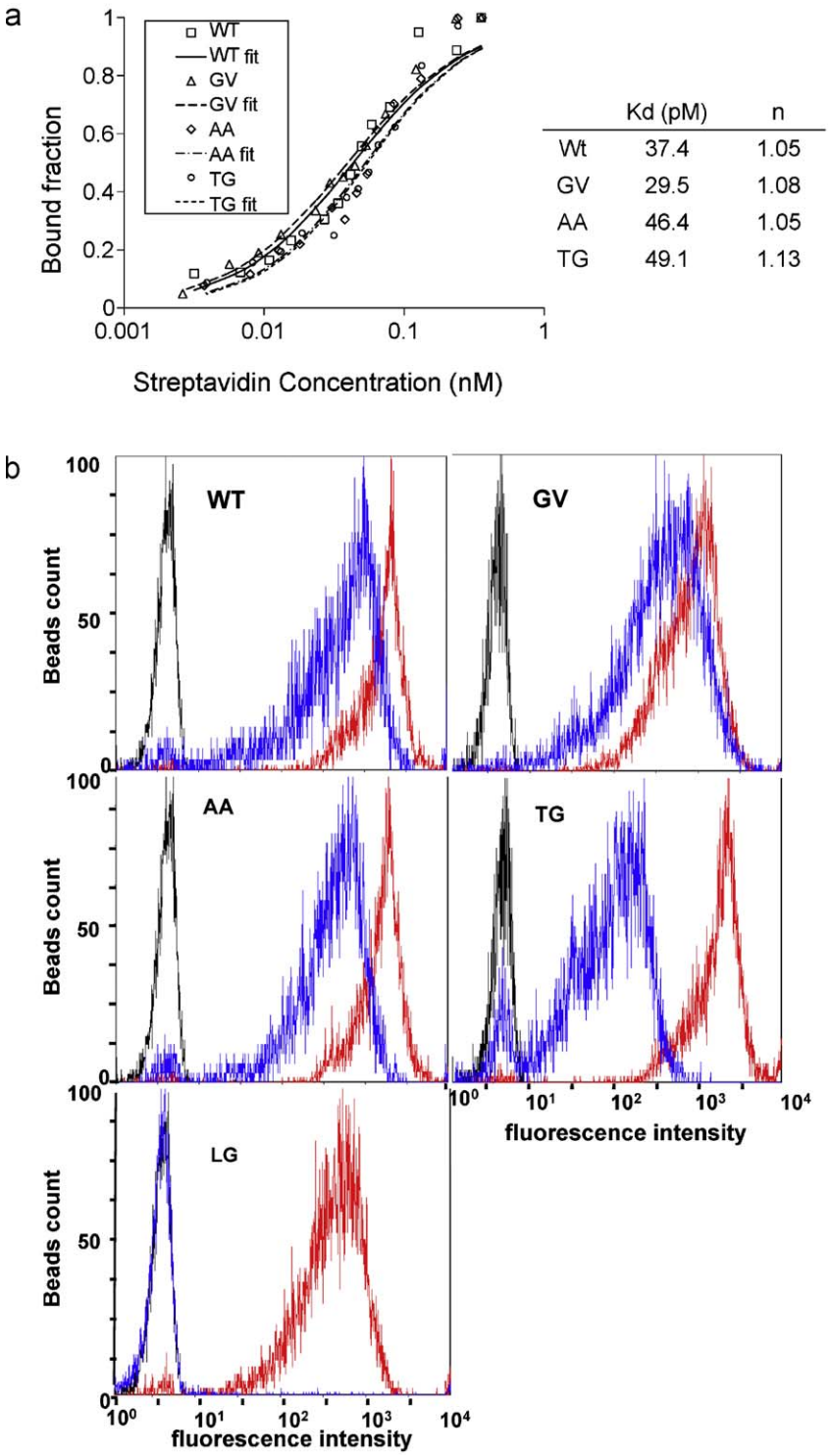

Fig. 8. (a) The binding affinity K_d of wt and mutant streptavidin for B4F was measured based on fluorescence quenching. The overlaid fits include optimized Hill coefficient n for each computed K_d. (b) Purified wt and mutant streptavidin were loaded on biotin beads, and the beads were fluorescently labeled using an antibody against the FLAG epitope at the C-terminus for analysis by flow cytometry (red). The same beads were also labeled using a biotinylated antibody and then labeled using fluorescently labeled secondary antibody (blue). Biotin beads without protein were labeled similarly as control (black).

To directly test this hypothesis, we re-purified LG in the presence of biotin. The CD spectrum of biotin-bound LG is similar to wt and is stable at temperatures above 80 °C (Fig. S7a). The beads-binding assay was also useful for characterizing the quaternary structure of the bound protein. For example, we labeled the immobilized protein using an unrelated biotinylated antibody. The biotinylated antibody binds the beads only if the immobilized streptavidin is an oligomer and has more than one biotin binding site. In contrast, the beads cannot be labeled using biotinylated antibody if the bound protein is a monomer. While the total amount of bound protein was similar for all mutants under saturating conditions, the binding of second biotin is reduced for TG and is absent for LG (Fig. 8b).

Therefore, the oligomer formation of these mutants is disrupted compared to wt.

4. Discussion

4.1. Errors caused by limited sampling

Since dynamic simulation can explore other energetically accessible conformations starting from a single structure, it can be useful for modeling the mutations that induce changes in the main chain conformation [17,18]. The problem that we investigated here is if dynamic simulation can be used to study how streptavidin dimerization would be affected by interfacial mutations. Because the residues at the dimer interface have high steric complementarity, a mutation that disrupts the side chain packing may destabilize subunit association without affecting the monomer structure. Our study shows simulation may have difficulty estimating the stability of a protein complex due to potentially incomplete equilibration. For example, some of the simulated mutants (TG and LG) clearly do not reach an equilibrium state after 10 ns although the total energy of the system reaches a stable value within 5 ns. The incomplete relaxation of the system and large fluctuations among simulated structures resulted in free energy calculation that are difficult to interpret and/or misleading. In contrast, if the interface stability is parameterized using the degree of solvation of the designed interface, it resulted in predictions that agree well with experiment. Although our study includes wt and only four mutants, the agreement between prediction and experiment is encouraging, given the simplicity and the physically intuitive nature of the model. The solvation parameter is computed based on structure, but it may be viewed as representing the dissociation process rather than the equilibrium state by describing the early steps of subunit dissociation rather than the final dissociated state. Therefore, our analysis suggests that interpreting the simulation as snapshots of an evolving system may be a useful way to estimate the stability of a protein complex.

In addition to inadequate equilibration, the simulated structures also contain large fluctuations that limit the accuracy of computed binding energy. In our simulations, these fluctuations occur with residues that are located far from the mutated residues (>10 Å), which should not correlate directly with the changes at the interface. Since most homology models do not consider contributions from distant residues, including only nearby atoms for the potential energy calculation appears to be an acceptable approximation. Since the computed energy depends on the cutoff value used to define neighboring atoms, we screened a range of values and examined how it changes the prediction. Using short cutoffs would leave out important interactions, whereas longer cutoffs may dilute the effect of mutation by including weakly coupled interactions. Either extreme would result in an inaccurate estimate of the mutational effects. We used a 8 Å cutoff in our calculation, because this value is sometimes used in the literature to define local interaction [52]. Although the resulting prediction that TG and LG are the two most unstable mutants qualitatively agrees with the experiment, it is important to note that the cutoff is an adjustable parameter and using a different value results in a different stability ranking among the constructs. One way to improve the accuracy of our free energy calculation is by optimizing the value of the dielectric constant ε, which requires the use of different ε values for polar and nonpolar residues [53]. Using residue-specific dielectric constants may have improved our binding energy calculation, but we did not implement variable dielectric constants for the dimer interface, since the benefits of fine tuning the dielectric constants are likely limited, given there are other larger sources of uncertainty, including large structural fluctuations.

4.2. Coupling to biotin binding

The interactions at the interface are the same in the simulations containing the full tetramer or a native dimer. Therefore, dimer association is not strongly coupled to tetramerization—at least within the time scale of our simulation. It also suggests that the native dimer is a distinct folding unit, since the interactions at the interface are not affected by other long distance domain–domain interactions. Despite limited sampling, we observe a clear correlation between biotin binding and dimer association. For example, biotin binding changes the side chain conformation of buried T91 as well as the orientation of the buried water Wat206, so that the hydrogen bonding patterns at the interface are different between the apo and complex structures (Fig. 2b and c). Wat206 is structurally important and likely contributes to the stability of the dimer, since a simulation that does not include the water results in structures that are qualitatively different from those included in the current study (data not shown). Therefore, a loss of water hydrogen bond in the apo structure may be a factor that contributes to reduced stability of apo streptavidin.

A correlation between the T91 side chain mobility and structural stability is further supported by the GV mutant, which is the only dimer in which the conformations of both T91 side chains remain as in the crystal structure. GV is also the only mutant that has higher stability than wt. In contrast, the other mutants, AA, TG, and LG all have similar side chain mobility as wt, and also have lower stability than wt. The increase in stability for GV may be due to the replacement of buried polar residues with isosteric nonpolar residues, which often stabilizes the molecule by increasing the hydrophobicity of the core [44,54,55] and reducing the entropic penalty of folding (Table 3). Regardless of the mechanism, the simulated structures of biotin-bound and apo streptavidin show that there is a correlation between the mobility of interface residues and experimentally measured dimer stability.

4.3. Interface design

One of the objectives in our study is to test if steric complementarity at the dimer interface can be redesigned. The mutants that we tested include the ones in which large (T76) and small (G74) residues are swapped (TG) or the side chain volume is redistributed (AA). Both mutants model the complementarity at the dimer interface based on a simple assumption that these residues interact only with each other. However, the contacts from neighboring residues are also likely to be important in determining steric complementarity. The TG dimer, which swaps the knob and hole residues, is unstable both because of a steric clash with A89 as well as the loss of water hydrogen bonds. Similarly, large steric repulsion between L74 of one subunit and A89/T91 of the other subunit appears to destabilize the LG dimer. The unfolding of LG, however, does not imply that the mutations directly interfere with the monomer folding, because the folding energy contribution from tetramerization, which is known to be important for stability, is missing in LG. This interpretation is supported by previous studies, which showed that streptavidin monomer and dimer are unstable unless additional mutations are introduced to replace solvent exposed hydrophobic residues [7,11]. Despite the disruptive interfacial mutations, adding biotin during LG refolding fully restores the tetrameric conformation (Fig. S7b). For example, the CD value at $\lambda = 216$ nm is 12% greater for LG-biotin than wt, showing that biotin binding can overcome destabilizing interfacial mutations and lead to folded monomer and oligomer structures (Fig. S7a).

To determine the melting temperature, we analyzed the transition at three different wavelengths, 205, 216, and 232 nm, because streptavidin has a significant number of disordered residues. For

example, the number of residues that form a β sheet (67 residues) is a small percentage of the entire protein (165 residues) [56], and the rest of the protein consists of either ordered or disordered loops. As such, the measured CD spectra show a strong negative peak around 205 nm. The positive peak around 230 nm suggests the presence of the poly(Pro)II helix with the main chain dihedrals (ϕ, ψ) = (−75°, +145°) [49,57]. The poly(Pro)II conformation is not unique to prolines, since glutamine, alanine, and glycine also have high poly(Pro)II helical propensity [58], and the conformation occurs frequently in various homopolymers and proteins with limited proline content [59]. Denaturing the poly(Pro)II helix either by a chaotropic salt treatment or by pH is known to reduce the positive peak intensity near 230 nm [57]. The streptavidin CD spectra at various temperatures show that the protein loses β sheet conformation (i.e. the minimum at 216 nm) and the poly(Pro)II helix peaks simultaneously, suggesting that the melting transition occurs globally and affects both β sheet and loop residues. To our knowledge, the use of a poly(Pro)II peak to measure the melting temperature of a globular protein has never been reported. But as TG measurements show, the use of noncanonical wavelengths in a CD analysis can be useful in some proteins with limited secondary structure.

Our binding measurements show that despite changes in stability, the mutants are functional and bind biotin with similar affinities as wt. Therefore, the interfacial mutations do not affect the quaternary structure that is relevant to the protein function. In addition to obtaining the binding affinity, we also analyzed the binding curve to determine if there is cooperativity between the binding sites. To this end, we determined the Hill coefficient by fitting the fraction bound to the following equation:

$$f_{bound} = \frac{[S]^n}{[S]^n + K_d} \tag{8}$$

The best fits were obtained for $n = 1.05–1.13$. Since a Hill coefficient greater than one suggests cooperativity among the binding sites, our data suggests that the ligand binding sites may be weakly cooperative. However, the low level of measured cooperativity does not fully resolve the conflicting reports in the literature, both arguing for and against cooperative biotin binding [60,61]. One possible mechanism by which different ligand binding sites communicate with each other is through structural tightening that result from the binding of B4F, which then propagates to other binding sites. It is important to note that since the binding of B4F involves both biotin–streptavidin interactions as well as interactions between fluorescein and streptavidin, biotin binding may have quantitatively different characteristics than B4F. That the fluorescence of B4F is quenched by nearly 9 fold upon binding suggests a close proximity of the fluorophore to an aromatic residue [29]. We observe that the fluorescence is unaffected if B4F is bound to a streptavidin monomer [11] containing the W120A mutation (data not shown), suggesting that W120 may be responsible for the observed fluorescence quenching of bound B4F.

The combination of simulation, modeling, and experiments presented here is significant for several reasons. First, the study characterizes the interactions at the native streptavidin dimer interface beyond what is available from the crystal structures. It also shows that MD can evaluate interfacial mutants for dimer association and help engineer novel streptavidin oligomers. While using MD as a general protein engineering tool remains challenging due to the computational complexity, analyzing the trajectories using a rationally designed metric can facilitate the design by accurately predicting the effects of interfacial mutations. The availability of a convenient and reliable computational tool to estimate the stability of a dimer will thus advance the discovery of other streptavidin mutants.

5. Conclusion

In this study, we used molecular dynamics simulation and biochemistry to model the streptavidin dimer interface and to evaluate how interfacial mutations affect its quaternary structure. The study shows that using energy calculation to predict the dimer stability is error prone due to significant structural fluctuations and uncertainties regarding the equilibrium structures. In contrast, parameterizing the dimer interface using a solvation parameter can predict if the mutant will form a stable complex. Simulated dynamics can thus help design streptavidin mutants that are difficult to analyze by the typical homology modeling and assist in the engineering of novel interface mutants.

Acknowledgements

This work was supported in part by the Interdisciplinary Research Development Fund from the University at Buffalo. The authors acknowledge the computational resources provided by the Center for Computational Research at UB and TeraGrid (Startup allocation No. MCB090190). We also acknowledge the Department of Pharmaceutical Sciences at UB for the use of spectrofluotometer and CD spectrometer (NIH Shared Instrument Grants S10-RR15877 and S10-RR013665).

Appendix A. Supplementary data

Supplementary data associated with this article can be found, in the online version, at doi:10.1016/j.jmgm.2010.09.009.

References

[1] W.A. Hendrickson, A. Pahler, J.L. Smith, Y. Satow, E.A. Merritt, R.P. Phizackerley, Crystal structure of core streptavidin determined from multiwavelength anomalous diffraction of synchrotron radiation, Proc. Natl. Acad. Sci. U.S.A. 86 (1989) 2190–2194.
[2] P.C. Weber, D.H. Ohlendorf, J.J. Wendoloski, F.R. Salemme, Structural origins of high-affinity biotin binding to streptavidin, Science 243 (1989) 85–88.
[3] S. Freitag, I. Le Trong, A. Chilkoti, L.A. Klumb, P.S. Stayton, R.E. Stenkamp, Structural studies of binding site tryptophan mutants in the high-affinity streptavidin–biotin complex, J. Mol. Biol. 279 (1998) 211–221.
[4] T. Sano, C.R. Cantor, Intersubunit contacts made by tryptophan 120 with biotin are essential for both strong biotin binding and biotin-induced tighter subunit association of streptavidin, Proc. Natl. Acad. Sci. U.S.A. 92 (1995) 3180–3184.
[5] A. Chilkoti, P.H. Tan, P.S. Stayton, Site-directed mutagenesis studies of the high-affinity streptavidin–biotin complex: contributions of tryptophan residues 79, 108, and 120, Proc. Natl. Acad. Sci. U.S.A. 92 (1995) 1754–1758.
[6] O.H. Laitinen, K.J. Airenne, A.T. Marttila, T. Kulik, E. Porkka, E.A. Bayer, et al., Mutation of a critical tryptophan to lysine in avidin or streptavidin may explain why sea urchin fibropellin adopts an avidin-like domain, FEBS Lett. 461 (1999) 52–58.
[7] T. Sano, S. Vajda, C.L. Smith, C.R. Cantor, Engineering subunit association of multisubunit proteins: a dimeric streptavidin, Proc. Natl. Acad. Sci. U.S.A. 94 (1997) 6153–6158.
[8] M. Gonzalez, C.E. Argarana, G.D. Fidelio, Extremely high thermal stability of streptavidin and avidin upon biotin binding, Biomol. Eng. 16 (1999) 67–72.
[9] M. Gonzalez, L.A. Bagatolli, I. Echabe, J.L. Arrondo, C.E. Argarana, C.R. Cantor, et al., Interaction of biotin with streptavidin thermostability and conformational changes upon binding, J. Biol. Chem. 272 (1997) 11288–11294.
[10] F.M. Aslan, Y. Yu, S.C. Mohr, C.R. Cantor, Engineered single-chain dimeric streptavidins with an unexpected strong preference for biotin-4-fluorescein, Proc. Natl. Acad. Sci. U.S.A. 102 (2005) 8507–8512.
[11] S.C. Wu, S.L. Wong, Engineering soluble monomeric streptavidin with reversible biotin binding capability, J. Biol. Chem. 280 (2005) 23225–23231.
[12] B.A. Katz, Binding of biotin to streptavidin stabilizes intersubunit salt bridges between Asp61 and His87 at low pH, J. Mol. Biol. 274 (1997) 776–800.
[13] B.A. Katz, R.T. Cass, In crystals of complexes of streptavidin with peptide ligands containing the HPQ sequence the pKa of the peptide histidine is less than 3.0, J. Biol. Chem. 272 (1997) 13220–13228.
[14] M. Karplus, J.A. McCammon, Molecular dynamics simulations of biomolecules, Nat. Struct. Biol. 9 (2002) 646–652.
[15] A.D. MacKerell, D. Bashford, M. Bellott, R.L. Dunbrack, J.D. Evanseck, M.J. Field, et al., All-atom empirical potential for molecular modeling and dynamics studies of proteins, J. Phys. Chem. B 102 (1998) 3586–3616.
[16] N. Chennamsetty, V. Voynov, V. Kayser, B. Helk, B.L. Trout, Design of therapeutic proteins with enhanced stability, Proc. Natl. Acad. Sci. U.S.A. 106 (2009) 11937–11942.

[17] S. Szep, S. Park, E.T. Boder, G.D. Van Duyne, J.G. Saven, Structural coupling between FKBP12 and buried water, Proteins 74 (2009) 603–611.
[18] S. Park, J.G. Saven, Statistical and molecular dynamics studies of buried waters in globular proteins, Proteins 60 (2005) 450–463.
[19] R.E. Hubbard, J.M. Thornton, NACCESS, University College London, Department of Biochemistry and Molecular Biology, 1993, p. Computer Program.
[20] L. Lo Conte, C. Chothia, J. Janin, The atomic structure of protein–protein recognition sites, J. Mol. Biol. 285 (1999) 2177–2198.
[21] L. Kale, R. Skeel, M. Bhandarkar, R. Brunner, A. Gursoy, N. Krawetz, et al., NAMD2: Greater scalability for parallel molecular dynamics, J. Comput. Phys. 151 (1999) 283–312.
[22] W. Humphrey, A. Dalke, K. Schulten, VMD: visual molecular dynamics, J. Mol. Graph. 14 (1996) 33–38.
[23] L.T. Chong, J.W. Pitera, W.C. Swope, V.S. Pande, Comparison of computational approaches for predicting the effects of missense mutations on p53 function, J. Mol. Graph. Model. 27 (2009) 978–982.
[24] N.A. Baker, D. Sept, S. Joseph, M.J. Holst, J.A. McCammon, Electrostatics of nanosystems: application to microtubules and the ribosome, Proc. Natl. Acad. Sci. U.S.A. 98 (2001) 10037–10041.
[25] I. Massova, P.A. Kollman, Computational alanine scanning to probe protein–protein interactions: a novel approach to evaluate binding free energies, J. Am. Chem. Soc. 121 (1999) 8133–8143.
[26] M. Howarth, D.J. Chinnapen, K. Gerrow, P.C. Dorrestein, M.R. Grandy, N.L. Kelleher, et al., A monovalent streptavidin with a single femtomolar biotin binding site, Nat. Methods 3 (2006) 267–273.
[27] W.J. Becktel, J.A. Schellman, Protein stability curves, Biopolymers 26 (1987) 1859–1877.
[28] J.K. Myers, C.N. Pace, J.M. Scholtz, Denaturant m values and heat capacity changes: relation to changes in accessible surface areas of protein unfolding, Protein Sci. 4 (1995) 2138–2148.
[29] G. Kada, H. Falk, H.J. Gruber, Accurate measurement of avidin and streptavidin in crude biofluids with a new, optimized biotin-fluorescein conjugate, Biochim. Biophys. Acta 1427 (1999) 33–43.
[30] G. Kada, K. Kaiser, H. Falk, H.J. Gruber, Rapid estimation of avidin and streptavidin by fluorescence quenching or fluorescence polarization, Biochim. Biophys. Acta 1427 (1999) 44–48.
[31] A.A. Bogan, K.S. Thorn, Anatomy of hot spots in protein interfaces, J. Mol. Biol. 280 (1998) 1–9.
[32] P. Chakrabarti, J. Janin, Dissecting protein–protein recognition sites, Proteins 47 (2002) 334–343.
[33] T. Clackson, J.A. Wells, A hot spot of binding energy in a hormone–receptor interface, Science 267 (1995) 383–386.
[34] T. Kajander, P.C. Kahn, S.H. Passila, D.C. Cohen, L. Lehtio, W. Adolfsen, et al., Buried charged surface in proteins, Structure 8 (2000) 1203–1214.
[35] C.N. Pace, Polar group burial contributes more to protein stability than nonpolar group burial, Biochemistry 40 (2001) 310–313.
[36] K. Takano, J.M. Scholtz, J.C. Sacchettini, C.N. Pace, The contribution of polar group burial to protein stability is strongly context-dependent, J. Biol. Chem. 278 (2003) 31790–31795.
[37] C.N. Pace, Energetics of protein hydrogen bonds, Nat. Struct. Mol. Biol. 16 (2009) 681–682.
[38] Y. Gebremichael, J.W. Chu, G.A. Voth, Intrinsic bending and structural rearrangement of tubulin dimer: molecular dynamics simulations and coarse-grained analysis, Biophys. J. 95 (2008) 2487–2499.
[39] C.F. Lopez, S.O. Nielsen, G. Srinivas, W.F. Degrado, M.L. Klein, Probing membrane insertion activity of antimicrobial polymers via coarse-grain molecular dynamics, J. Chem. Theory Comput. 2 (2006) 649–655.
[40] J.D. Perlmutter, J.N. Sachs, Experimental verification of lipid bilayer structure through multi-scale modeling, Biochim. Biophys. Acta 1788 (2009) 2284–2290.
[41] F. Crick, The packing of [alpha]-helices: simple coiled-coils, Acta Crystallogr. 6 (1953) 689–697.
[42] T.B. Fischer, J.B. Holmes, I.R. Miller, J.R. Parsons, L. Tung, J.C. Hu, et al., Assessing methods for identifying pair-wise atomic contacts across binding interfaces, J. Struct. Biol. 153 (2006) 103–112.
[43] R.I. Litvinov, O.V. Gorkun, S.F. Owen, H. Shuman, J.W. Weisel, Polymerization of fibrin: specificity, strength, and stability of knob–hole interactions studied at the single-molecule level, Blood 106 (2005) 2944–2951.
[44] D.W. Sammond, Z.M. Eletr, C. Purbeck, B. Kuhlman, Computational design of second-site suppressor mutations at protein–protein interfaces, Proteins 78 (2010) 1055–1065.
[45] T.E. Creighton, Proteins Structure and Molecular Properties, Second ed., W.H. Freeman and Company, New York, 1993.
[46] E.L. Humphris, T. Kortemme, Prediction of protein–protein interface sequence diversity using flexible backbone computational protein design, Structure 16 (2008) 1777–1788.
[47] S. Miyamoto, P.A. Kollman, Absolute and relative binding free energy calculations of the interaction of biotin and its analogs with streptavidin using molecular dynamics/free energy perturbation approaches, Proteins 16 (1993) 226–245.
[48] N. Sreerama, R.W. Woody, Computation and analysis of protein circular dichroism spectra, Methods Enzymol. 383 (2004) 318–351.
[49] D.M. John, K.M. Weeks, van't Hoff enthalpies without baselines, Protein Sci. 9 (2000) 1416–1419.
[50] M.J. Waner, D.P. Mascotti, A simple spectrophotometric streptavidin–biotin binding assay utilizing biotin-4-fluorescein, J. Biochem. Biophys. Methods 70 (2008) 873–877.
[51] N.M. Green, Avidin and streptavidin, Methods Enzymol. 184 (1990) 51–67.
[52] S.A. Marshall, S.L. Mayo, Achieving stability and conformational specificity in designed proteins via binary patterning, J. Mol. Biol. 305 (2001) 619–631.
[53] I.S. Moreira, P.A. Fernandes, M.J. Ramos, Computational alanine scanning mutagenesis—an improved methodological approach, J. Comput. Chem. 28 (2007) 644–654.
[54] C.D. Waldburger, J.F. Schildbach, R.T. Sauer, Are buried salt bridges important for protein stability and conformational specificity? Nat. Struct. Biol. 2 (1995) 122–128.
[55] V.V. Loladze, D.N. Ermolenko, G.I. Makhatadze, Thermodynamic consequences of burial of polar and non-polar amino acid residues in the protein interior, J. Mol. Biol. 320 (2002) 343–357.
[56] W. Kabsch, C. Sander, Dictionary of protein secondary structure: pattern recognition of hydrogen-bonded and geometrical features, Biopolymers 22 (1983) 2577–2637.
[57] A.L. Rucker, T.P. Creamer, Polyproline II helical structure in protein unfolded states: lysine peptides revisited, Protein Sci. 11 (2002) 980–985.
[58] M.A. Kelly, B.W. Chellgren, A.L. Rucker, J.M. Troutman, M.G. Fried, A.F. Miller, et al., Host–guest study of left-handed polyproline II helix formation, Biochemistry 40 (2001) 14376–14383.
[59] A. Toumadje, W.C. Johnson, Systemin has the characteristics of a poly(L-Proline)-II type helix, J. Am. Chem. Soc. 117 (1995) 7023–7024.
[60] T. Sano, C.R. Cantor, Cooperative biotin binding by streptavidin electrophoretic behavior and subunit association of streptavidin in the presence of 6 M urea, J. Biol. Chem. 265 (1990) 3369–3373.
[61] M.L. Jones, G.P. Kurzban, Noncooperativity of biotin binding to tetrameric streptavidin, Biochemistry 34 (1995) 11750–11756.